

# SUBSURFACE TARGET IMAGING USING A MULTI-RESOLUTION 3D QUADTREE ALGORITHM

Ali Cafer Gürbüz , James H. McClellan and Waymond R. Scott Jr.

Georgia Institute of Technology  
Atlanta, GA 30332-0250;

## ABSTRACT

The imaging of subsurface targets, such as landmines, using Ground Penetrating Radar (GPR) is becoming an increasingly important area of research. Conventional image formation techniques expend large amounts of computational resources on fully resolving a region, even if there is a large amount of clutter. For example, standard backprojection algorithms require  $O(N^3)$ . However, by using multi-resolution techniques - such as quadtree - potential targets and clutter can be discriminated more efficiently with  $O(N^2 \log_2 N)$ . Because prior work has focused on the imaging of surface targets, quadtree techniques have mostly been developed for 2D imaging. Target depth adds another dimension to the imaging problem; therefore, we have developed a 3D quadtree algorithm. In this case, the mine field is modeled as a volume that is sub-divided at each stage of the quadtree algorithm. From each of these sub-volumes, the energy intensity is calculated. As the algorithm proceeds to finer resolutions, the energy in region containing a potential target increases, while that of background noise decreases. A multi-stage detector applied on intermediate quadtree data uses this change in energy to discriminate between regions of targets and clutter. This is advantageous because only the regions containing likely targets are investigated by additional sensors that are relatively slow in comparison to GPR (e.g. seismic or EMI sensors). This algorithm is tested on synthetic and experimental data collected from a model mine field at Georgia Institute of Technology. Even under near field and small aperture conditions, which hold for the mine detection case, test results show that target location information can be gathered with processing using the 3D quadtree algorithm.

**Keywords:** Quadtree Backprojection, Subsurface Imaging, 3D Imaging, Mine Detection, Ground Penetrating Radar

## 1. INTRODUCTION

Synthetic aperture ground penetrating radar (GPR) techniques have been extremely useful in the imaging and detection of subsurface targets. Applications include the investigation of shallow geological and engineering features on land and detection and imaging of subsurface land mines, which is the focus of this paper.

As the GPR antenna scans a region, the radar transmits and receives a series of pulses. The impulse response of such a synthetic aperture radar (SAR) is a spatially variant hyperbolic curve in the space-time domain. There are a variety of methods for combining the received echoes into an image; e.g. standard backprojection,<sup>2,5</sup> or Fourier domain SAR<sup>2,5</sup> image formation. All of these methods process the entire region of interest to make a detection decision. On the other hand, quadtree backprojection is a multi-resolution technique that uses a divide-and-conquer processing approach. At each stage, space-time imaging is first performed over a number of sub-patches separately. As the quadtree algorithm iterates, increasingly finer sub-patches of the scene are resolved. Detection of potential targets can be accomplished without fully resolving the entire scene.<sup>2,4</sup> Thus, relative to standard backprojection, this method provides comparable results with increased computational efficiency.

---

Further author information: (Send correspondence to Ali Cafer Gürbüz):

A. C. Gürbüz: E-mail: alicaffer@ece.gatech.edu, Telephone: 404-894-2977

J. H. McClellan: E-mail: jim.mcclellan@ece.gatech.edu, Telephone: 404-894-8325

W. R. Scott: E-mail: waymond.scott@ece.gatech.edu, Telephone: 404-894-3048

Previous work has mostly focused on developing quadtree algorithms for imaging surface targets.<sup>2,4</sup> Subsurface target imaging adds a third dimension to the problem. Thus, we extend the quadtree approach to a three dimensional algorithm that handles volumes rather than surfaces. Quadtree methods are especially effective for far field and large aperture conditions; however, neither of the conditions exist in the mine detection problem. Nevertheless, results from computer-generated data, as well as experimental data measured at model mine fields at Georgia Institute of Technology, show that the 3D quadtree algorithm developed still provides useful target location information under these conditions.

First, the basic theory of backprojection and the 3D quadtree imaging/detection algorithm is presented in Section 2. Synthetic and experimental data results are shown in Section 3.

## 2. BASIC THEORY

### 2.1. Standard Backprojection

Standard Backprojection(STBP) is a space-time domain algorithm that performs matched filtering of the synthetic aperture radar (SAR) for each point in the space domain. SAR is an imaging technique in which the radar antenna is moved over the region being imaged to emulate a physically larger aperture. The impulse response of the SAR data acquisition process is a spatially variant hyperbolic curve. The STBP algorithm implements the matched filtering as a coherent summation along all such hyperbolas for every pixel in the image. For an infinite aperture path, the STBP<sup>2,5</sup> can be mathematically represented as:

$$f(x_n, y_n) = \int_{-\infty}^{\infty} \int_{-\infty}^{\infty} w(u) d(u, t) \delta(t - \frac{2}{c} \sqrt{x_n^2 + (y_n - u)^2}) dt du, \quad (1)$$

where  $d(u, t)$  is the SAR space-time domain data,  $w(u)$  is the aperture weighting function and  $f(x_n, y_n)$  is the reconstructed image.

STBP is a computationally complex algorithm. For 2D processing of an  $N \times N$  image with  $N$  sensors, the algorithm performs  $O(N^3)$  computations. For 3D processing of an  $N \times N \times N$  volume with  $N^2$  sensors, the computational complexity increases to  $O(N^5)$ . On the other hand, quadtree backprojection attains much more efficient results, requiring  $N^2 \log_2 N$  computations<sup>1</sup> for the 2D case, and  $N^3 \log_2 N$  for the 3D case.

### 2.2. 3D Quadtree Backprojection

Despite all the advantages of standard backprojection, it is rarely used because of its high computational complexity. The quadtree backprojection algorithm<sup>1</sup> was introduced as a fast approximation to backprojection. The standard quadtree algorithm divides the scene into sub-patches, combines the aperture points, and defines the intermediate stage beam data for each patch and aperture point at each stage. In this way, at each stage a finer resolution of the scene is obtained. The quadtree algorithm is illustrated in Fig. 1 for the 2D case.

The standard quadtree algorithm just described operates on areas and is thus only applied to surface imaging. Subsurface imaging problems, i.e. the imaging of land mines, are three dimensional. Thus, the quadtree approach is extended to a three dimensional algorithm that handles volumes rather than surfaces.

Quadtree methods are based on a divide and conquer approach. A general divide and conquer strategy can be applied simultaneously to both image patches and aperture points when dividing by small integers  $P, Q$  (i.e.  $P = 2$  and  $Q = 2$  in radix-2 case). In each iteration following operations are performed by the 3D quadtree algorithm:

- *Partitioning of Imaged Region:* A volume is divided into  $Q \times Q \times Q$  cubic sub-volumes. In this way  $Q^3$  new sub-volume centers are defined at every iteration stage.  $\Delta_x^i, \Delta_y^i$  and  $\Delta_z^i$  are defined as the sub-volume size parameters in the  $i^{th}$  stage; the size parameters of the sub-volumes in  $(i + 1)^{th}$  stage are defined as follows:

$$\Delta_x^{i+1} = \frac{\Delta_x^i}{Q} \quad \Delta_y^{i+1} = \frac{\Delta_y^i}{Q} \quad \Delta_z^{i+1} = \frac{\Delta_z^i}{Q} \quad (2)$$

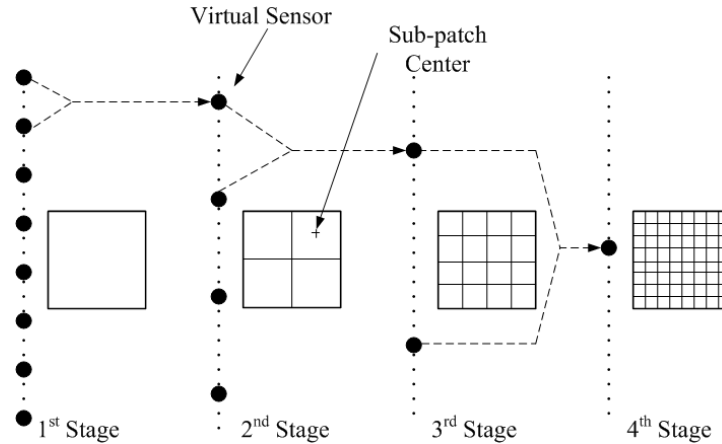


**Figure 1.** Quadtree algorithm structure for the radix-2 case.

In the radix-2 case, where  $P = 2$  and  $Q = 2$ , this yields 8 sub-volumes. Because of this, it would perhaps be more appropriate to call this structure “oct-tree”. However, since the term “quadtree” has come to be used to indicate a generic class of tree-structures, we will continue to use this terminology throughout this paper, even for the 3D case.

- *Combination of Aperture Points:* The quadtree algorithm contains combination of parent nodes to form virtual aperture points. In standard quadtree algorithm for radix-2 case this is done by combining two neighboring nodes since there is one line of aperture points. In subsurface imaging problem the aperture points are designated over the surface to be imaged and there are many possible ways to group them. As an initial choice, we decided to form a single virtual sensor from each  $P$  by  $P$  group of parent sensors. The location of the virtual sensor is then given by the coordinates of the center of the  $P \times P$  square where the corners are defined by the parent sensor coordinates. This is illustrated in Figure 2
- *Child Sensor Data Regeneration:* The main task of the 3D quadtree algorithm is generating data from the parent sensors of the child nodes for each sub-volume. At each iteration, beam data for newly updated virtual sensors are generated for each sub-volume using the data of the parent sensors. The portions of parent sensor data that correspond to the time when the signal enters and leaves the sub-volume, are coherently summed to form the child sensor data for that particular sub-volume. Child sensor data generation is illustrated in Figure 2. The time at which the equivalent data segment begins or ends is determined by the travel time between the virtual (child) sensor and the sub-volume. Thus, the calculation of these travel times is a critical part of the quadtree algorithm, and is discussed next.

Travel times of the waves from the sensors to the sub-volumes are determined not only by the distances between them but also the wave path in the medium. In sub-surface imaging the wave travels through two different mediums, air and ground. In general, when an electromagnetic pulse encounters the boundary between two different media, the propagation direction changes according to Snell’s law. When we consider near-field imaging problems such as mine detection this issue becomes more important since the distance between antenna and target is relatively small. The exact calculation of the refraction point requires the solution of a 4<sup>th</sup> degree polynomial. Instead an approximate solution for the refraction point<sup>3</sup> is used and shown in Eq. 3, as illustrated in Fig. 3:

$$x_2 \approx x_3 + \sqrt{\frac{\varepsilon_1}{\varepsilon_2}}(x_1 - x_3) \quad (3)$$

In order to have uniform segments for the data, a spherical approximation is applied to the cubic sub-volumes. In this way, cubic sub-volumes are modelled as spheres encompassing the corners of the sub-volume. The radius

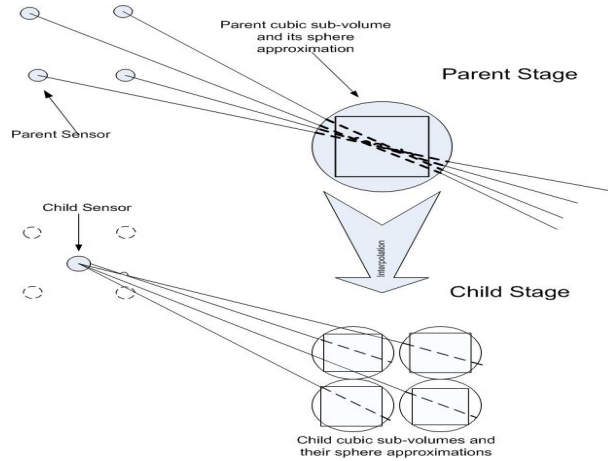


**Figure 2.** Child data generation. 4 of 8 child sub-volumes are illustrated

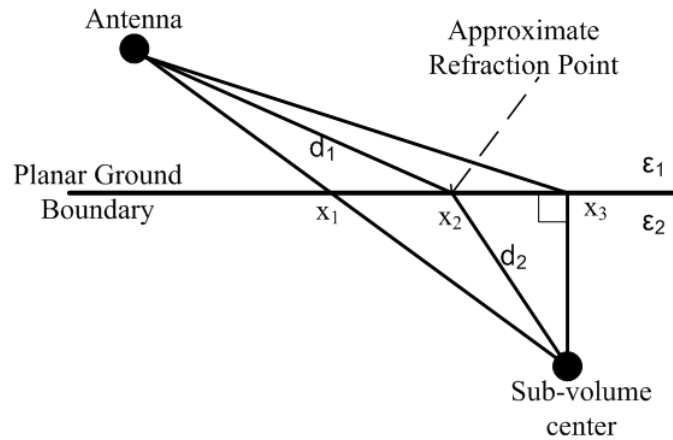


**Figure 3.** Determination of approximate refraction point.

of the sphere at the  $i^{th}$  stage is determined by the sub-volume size parameters  $\Delta R_i = \sqrt{(\Delta x^i)^2 + (\Delta y^i)^2 + (\Delta z^i)^2}$  and the radius of the spheres for the consecutive stages are related by  $\Delta R_{i+1} = \Delta R_i/Q$ .

The one-way travel times for the wave to enter and leave the sub-volume can be found by Eq.4 and Eq.5.

$$t_{start} = \frac{d_1}{c} + \frac{d_2 - \Delta R}{v} \quad (4)$$

$$t_{stop} = \frac{d_1}{c} + \frac{d_2 + \Delta R}{v} \quad (5)$$

In Eq.4 and Eq.5  $d_1$  and  $d_2$  are distances from the approximate refraction point to the sensor and sub-volume center respectively, as illustrated in Fig. 3.  $\Delta R$  is the radius of the spherical approximation of the sub-volume. the parameters  $v$  and  $c$  are the wave velocity in ground and air respectively. Here it is important to note that the velocity of the wave in the ground is assumed to be constant throughout the medium. Actually the velocity of propagation is affected by different sources, such as changes in permittivity, the type of soil, and ground conductivity. In our calculations in Section 3 a dry sand model with permittivity  $\epsilon_2 = 4$  is utilized.

Using Eq.4 and Eq.5, the segments of the data that correspond to entering and leaving the sub-volume can be identified. The next step is to combine the data of parent sensors to generate the data of child sensors. The child node beam data is generated by a coherent summation of the parent node data segments. Child sensor data generation illustrated in Figure 2 and is formulated next.

The data at the  $i^{th}$  stage is represented by  $d_i(s_x, s_y, t, \xi, \eta, \kappa)$ , where  $s_x$  and  $s_y$  represent spatial sensor positions given a fixed elevation,  $\xi, \eta$ , and  $\kappa$  indicate center coordinates of the sub-volumes; and  $t$  represents the fast time. Using this data representation, child node data to any particular sub-volume can be expressed as follows:

$$d_{i+1}[s_{x_C}, s_{y_C}, t_C, \xi_C, \eta_C, \kappa_C] = \sum_{s_x=s_{x_P}}^{s_{x_P}+1} \sum_{s_y=s_{y_P}}^{s_{y_P}+1} d_i[s_x, s_y, t, \xi_P, \eta_P, \kappa_P] W_{\xi_C, \eta_C, \kappa_C}[[t - \Delta R_{i+1}]]. \quad (6)$$

where  $d_{i+1}[s_{x_C}, s_{y_C}, t_C, \xi_C, \eta_C, \kappa_C]$  is  $(i+1)^{th}$  data of the child,  $d_i[s_x, s_y, t, \xi_P, \eta_P, \kappa_P]$  is the parent data at the  $i^{th}$  stage, and  $W_{\xi_C, \eta_C, \kappa_C}[t]$  is a time-domain windowing function corresponding to the appropriate segment of the parent data.

To obtain an image of the subsurface volume, the energy in each sub-volume is defined as in Equation 7.

$$E_i(\xi, \eta, \kappa) = \sum_{s_x} \sum_{s_y} \sum_t d(s_x, s_y, t, \xi, \eta, \kappa)^2 \quad (7)$$

In Equation 7  $E_i(\xi, \eta, \kappa)$  is the energy of the sub-volume centered at  $(\xi, \eta, \kappa)$  at the  $i^{th}$  stage. By defining the intensity of each pixel as the energy for each sub-volume in different stages, a multi-resolution 3D image which has a finer resolution at each stage is obtained. The image of quadtree stage is the scanned by a detection and region elimination algorithm, as explained next.

### 2.3. Detection and Region Elimination

The purpose of detection is to distinguish regions containing coherent scatterers, such as mines, from other regions consisting of only clutter. The detector exploits the fact that from stage to stage, the energy for a coherent target increases relative to the total energy, while the energy of background noise and clutter decreases. Such energy differentials are exploited by defining a probability mass function (pmf) based on the ratio of the energy in a sub-volume ( $s_{i+1}$ ) to that in its parent ( $s_i$ ):

$$P(s_{i+1}|s_i) = \frac{E(s_{i+1})}{E(s_i)} \quad (8)$$

The probability of a target being present at a subvolume in the stage  $i+1$  is then given by Bayes Rule as

$$P(s_{i+1}) = P(s_{i+1}|s_i) \cdot P(s_i|s_{i-1}) \cdots P(s_1). \quad (9)$$

Thus, the probability for a target present is associated with every subvolume at the finest resolution of the quadtree. When no target is present, subsurface ground clutter measurements show that the noise is non-uniform. Nevertheless, for simplicity we used a Gaussian white noise approximation for the noise distribution. The generalized likelihood ratio test (GLRT) then takes the form

$$\frac{P(s_i)}{P_n(n)} \geq \gamma \quad (10)$$

where  $\gamma$  is a constant threshold.

### 3. EXPERIMENT AND RESULTS

#### 3.1. Ground Reflection Removal (GRR)

Reflection of the transmitted wave from the ground is a major obstacle in the imaging of subsurface targets. These reflections are higher in amplitude than any mine reflection and may result in unwanted artifacts in the focused image if it is not removed prior to signal processing. Before applying the quadtree algorithm ground reflections are removed. To do this, first a ground reflection model is generated by averaging the experimental data from the sandbox where it is known apriori no target is present. The experimental ground reflection model is illustrated in Fig. 4a.

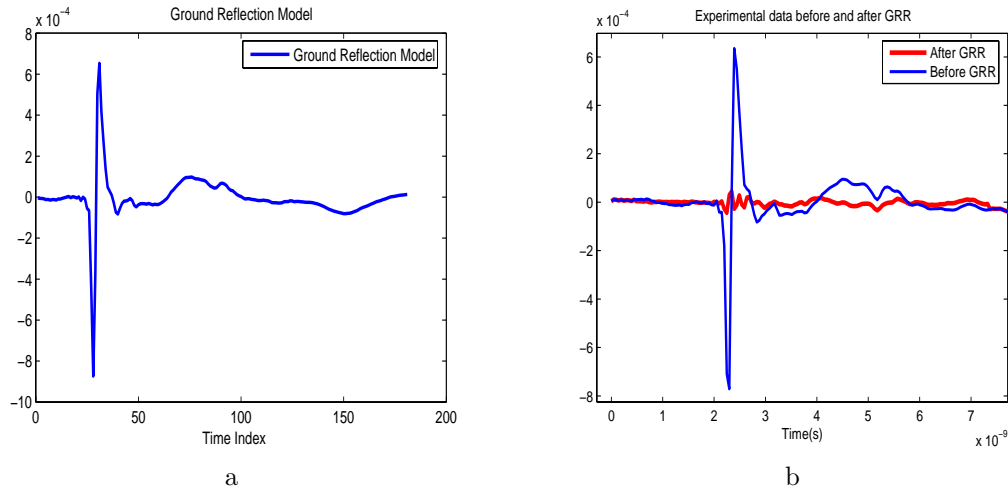


Figure 4. a) Ground Reflection Model b)One A-scan before and after GRR.

The ground reflection model is correlated with the returns at each measurement point to determine their relative lag. An appropriately delayed version of the model is then subtracted from the measurement. One example of experimental A-scan data is shown in Fig. 4b, before and after GRR. As can be observed the magnitude of the ground reflections are greatly reduced. Figure 5 shows a line scan over two anti-personal (AP) and one anti-tank (AT) mine before and after GRR. Again mine reflections can be seen clearer after GRR.

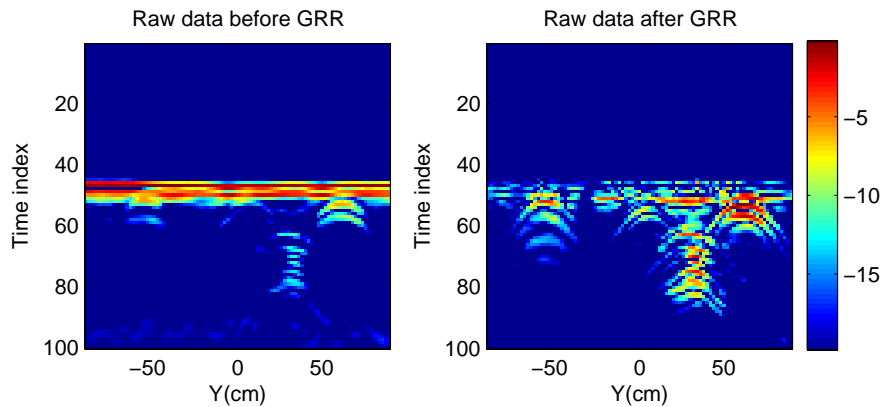
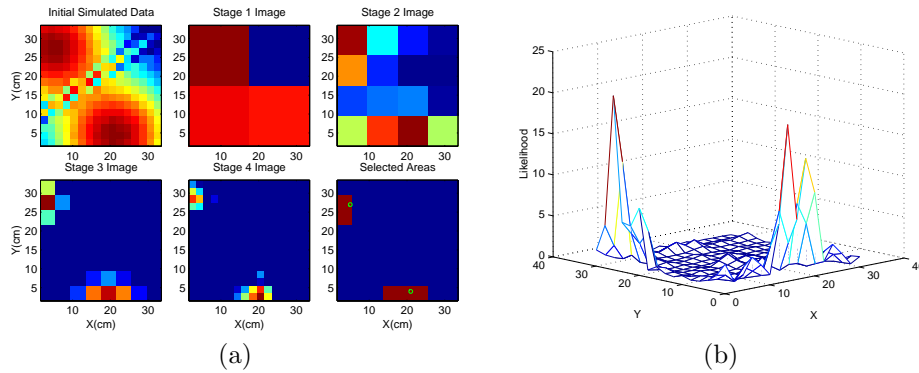


Figure 5. Experimental Line Image Before and After GRR.

### 3.2. Synthetic Data Results

To test the 3D quadtree algorithm on a variety of system specifications (such as aperture size, antenna height, the transmitter-receiver distance, target depth, soil type, and antenna step size) a GPR synthetic data generation program is developed. Here, we present the results for two synthetic data examples.

**Example 1.** In this scenario, the search area is a 32cm x 32cm square. The system configuration is as follows: aperture size = 16; antenna height = 20 cm; transmitter-receiver distance = 5 cm; step size = 2cm; and soil type = dry sand with dielectric permittivity  $\epsilon = 4$ . There are two point targets in the sand buried at positions (21,4,-20) and (5,27,-20). Figure 6a shows an overhead view the result of the quadtree algorithm at different stages with the energy underneath the surface integrated to form the flattened images. Both targets are captured correctly by the algorithm and 92.2% of the surface area is eliminated from further investigation by other sensors or imaging algorithms. Figure 6b shows the likelihood function over the surface defined in Eq.9.



**Figure 6.** (a)Quadtree stages for synthetic data Ex.1 (b) Likelihood distribution over the surface

**Example 2.** A single target is placed at a position (13,10,-10). All system parameters are the same as before, except that now the antenna height is 10 cm and the step size is 1 cm. Figure 7 shows the results with three-dimensional views. It can be seen from the Figure 7 that with this method not only x and y coordinates but also the depth information about the target can be obtained. In this case, the target is twice as close as in the first example, yet 93% of the volume has been eliminated from further investigation. This corroborates the performance of the quadtree algorithm under near-field conditions.

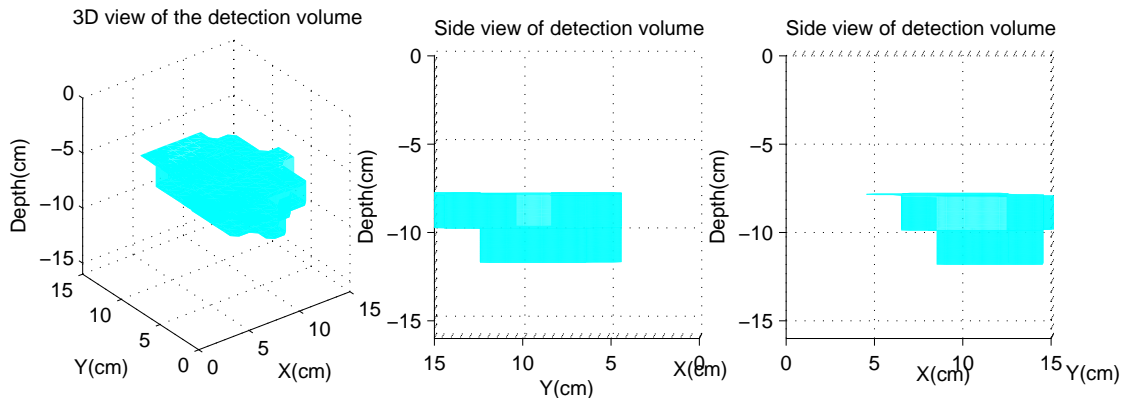


**Figure 7.** 3D view of results for synthetic data Ex. 2..

### 3.3. Experimental Data Results

The 3D quadtree algorithm was tested on the data obtained from the model mine field at Georgia Institute of Technology using varying kinds of AP and AT mines as well as different sources of clutter. The targets are buried according to the burial map shown in Figure 8(b).<sup>6</sup> The targets used in this experiment are listed with their corresponding properties in Table 1 and the picture of the targets are shown in Figure 8(a).<sup>6</sup> The experiment parameters are as follows: Phase centers of transmitter and receiver antennas are at 27.8 cm height, transmitter-receiver distance is 12 cm, antenna step size is 2 cm. The GPR antenna scans over 1.8 m x 1.8 m region giving a 91x91 measurements.

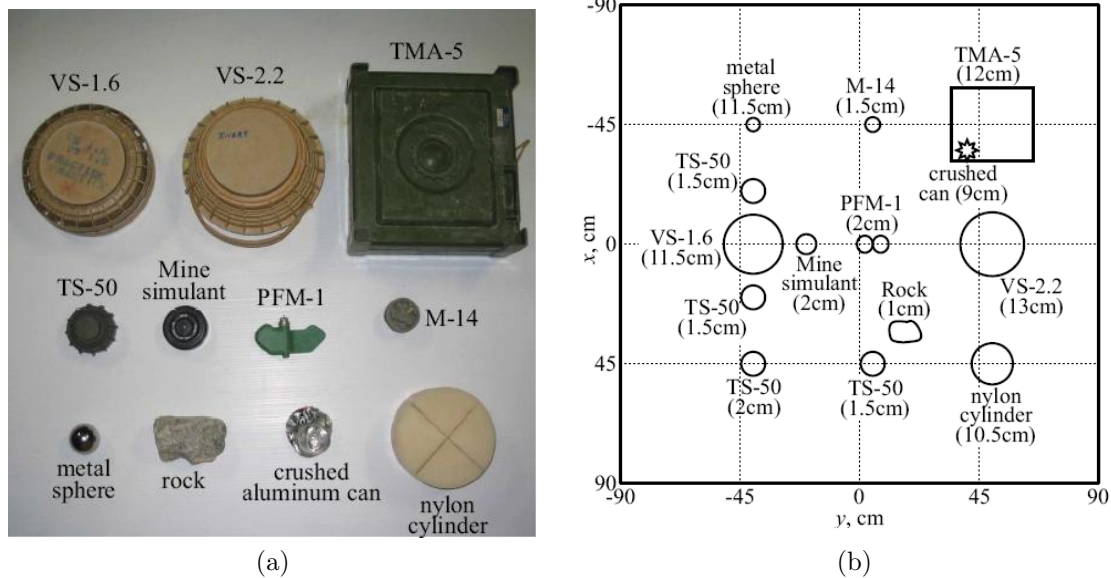


**Figure 8.** (a) Picture of the buried targets and (b) Burial map of the targets in sand. The numbers in the parentheses are the buried depths of the targets.

**Table 1.** Summary of Target Properties. In the dimensions column, L, W, D, and H represent length, width, diameter, and height, respectively. The target dimensions are shown in centimeters.<sup>6</sup>

target	type	material	dimensions (cm)
VS-1.6	anti-tank	plastic	22.2 (D), 9.2 (H)
VS-2.2	anti-tank	plastic	24.0 (D), 12.0 (H)
TMA-5	anti-tank	plastic	31.2 (L), 27.5 (W), 11.3 (H)
TS-50	anti-personnel	plastic	9.0 (D), 4.5 (H)
PFM-1	anti-personnel	plastic	11.9 (L), 6.4 (W), 2.0 (H)
M-14	anti-personnel	plastic	5.6 (D), 4.0 (H)
mine simulant	simulant	plastic	7.5 (D), 3.8 (H)
metal sphere	clutter	aluminum	5.1 (D)
rock	clutter	rock	12.0 (L), 8.0 (W), 7.5 (H)
crushed coke can	clutter	aluminum	8.0 (D), 3.0 (H)
nylon cylinder	clutter	nylon	15.5 (D), 7.6 (H)

Antenna aperture is not so large as to cover all the scan region. 3D Quadtree algorithm is applied to 32cm x 32cm regions and the results are concatenated accordingly. The detection algorithm is applied to the first three

stages of the 3D quadtree algorithm and the result is shown in Figure 9.

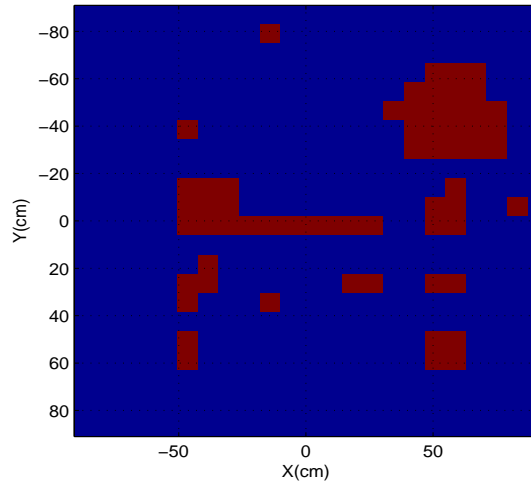


**Figure 9.** Detection areas for the burial scenario shown in Figure 8

It can be observed from the Figure 9 that the detection algorithm captured most of the targets successfully and eliminated a significant part of the total area from further investigation of processing algorithms and other sensors. The next set of results is an example of reflections over an AP mine.

Figure 10 shows the quadtree algorithm applied on raw data measured over a VS-50 AP mine buried 1.3 cm deep. The height of the GPR transmitter and receiver is 11.43 cm, with a separation distance of 11.5 cm. With a step size of 2 cm, at this height the antennas have approximately a 16 point aperture length.

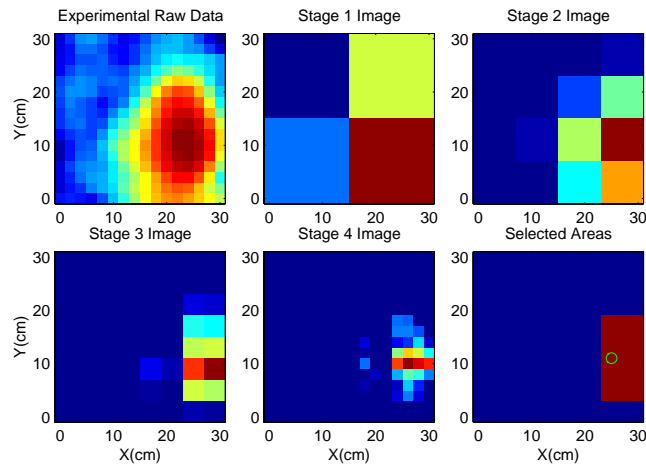


**Figure 10.** Overhead view of experimental data over VS-50 mine.

In this case, the object is very close to the ground; thus we are operating under low aperture size and very near-field conditions. Despite this, we were still able to locate the mine and eliminate 87.5% of the region from consideration.

## 4. CONCLUSION

In this paper we have developed and verified the performance of a 3D quadtree backprojection algorithm for application to the detection and imaging of land mines. In particular, our results from both computer simulations and processing experimental data show that target location information can be generally extracted even under small aperture and near-field conditions. Better ground reflection removal techniques and more suitable interpolation of the parent sensor data will increase the efficiency of the algorithm. By applying a computationally efficient 3D quadtree algorithm, we have developed method of using a fast sensor like GPR to prescreen a region and separate clutter from potential target locations. When additional, slower sensors - such as seismic sensors - are also used in conjunction with the GPR, overall time requirements can be reduced by applying the slower sensors only to the probable target regions identified by the quadtree algorithm. We plan to further pursue such sensor fusion issues in future work.

## ACKNOWLEDGMENTS

This work is supported under MURI by the U.S. Army Research Office under contract number DAAD19-02-1-0252

## REFERENCES

1. J. McCorkle, and M. Rofheart, "An order  $n^2 \log n$  backprojector algorithm for focusing wide-angle wide-bandwidth arbitrary motion synthetic aperture radar," *Proc. of SPIE*, vol. 2747, pp. 25-36, 1996.
2. S-K. Oh, "Iterative space-time domain fast multiresolution SAR imaging algorithms," *Ph.D. Thesis, Georgia Institute of Technology*, 2001.
3. E. M. Johansson, and J. E. Mast, "Three dimensional ground penetrating radar imaging using a synthetic aperture time-domain focusing," *In Proc. of SPIE Conference on Advanced Microwave and Millimeter Wave Detectors*, vol. 2275, pp. 205-214, 1994.
4. L. M. Kaplan, J. H. McClellan, and S-K. Oh, "Prescreening During Image Formation for Ultrawideband Radar," *IEEE Trans. On Aerospace and Electronic Systems*, vol. 38, no. 1, pp. 74-88, 2002.
5. Mehrdad Soumekh, "Synthetic Aperture Radar Signal Processing with Matlab Algorithms", *John Wiley and Sons Inc.*, 1999
6. Kangwook Kim, Ali Cafer Gurbuz, Waymond R. Scott, Jr. and James H. McClellan, "A Multi-Static Ground-Penetrating Radar with an Array of Resistively-Loaded Vee Dipole Antennas for Landmine Detection," in *Detection and Remediation Technologies for Mines and Minelike Targets X*, Proc. SPIE, 2005